Chinese Chemical Letters 36 (2025) 109589

Contents lists available at ScienceDirect

Chinese Chemical Letters

journal homepage: www.elsevier.com/locate/cclet

Emerging natural clay-based materials for stable and dendrite-free lithium metal anodes: A review

Haobo Wang[a], Fei Wang[b], Yong Liu[a,c,*], Zhongxiu Liu[a], Yingjie Miao[a], Wanhong Zhang[a], Guangxin Wang[a], Jiangtao Ji[d,*], Qiaobao Zhang[e,*]

[a] School of Materials Science and Engineering, Provincial and Ministerial Co-construction of Collaborative Innovation Center for Non-ferrous Metal new Materials and Advanced Processing Technology, Henan University of Science and Technology, Luoyang 471023, China
[b] Faculty of Engineering, Huanghe Science and Technology University, Zhengzhou 450063, China
[c] Henan Key Laboratory of Non-Ferrous Materials Science & Processing Technology, Henan University of Science and Technology, Luoyang 471023, China
[d] College of Agricultural Equipment Engineering, Henan University of Science and Technology, Luoyang 471023, China
[e] State Key Laboratory of Physical Chemistry of Solid Surfaces, College of Materials, Xiamen University, Xiamen 361005, China

ARTICLE INFO

Article history:
Received 9 January 2024
Revised 21 January 2024
Accepted 29 January 2024
Available online 4 February 2024

Keywords:
Natural clay-based materials
Aolid-state electrolyte
Surface modification
Li metal anodes
Rechargeable batteries

ABSTRACT

Lithium metal is one of the most promising anodes for lithium batteries because of their high theoretical specific capacity and the low electrochemical potential. However, the commercialization of lithium metal anodes (LMAs) is facing significant obstacles, such as uncontrolled lithium dendrite growth and unstable solid electrolyte interface, leading to inferior Coulombic efficiency, unsatisfactory cycling stability and even serious safety issues. Introducing low-cost natural clay-based materials (NCBMs) in LMAs is deemed as one of the most effective methods to solve aforementioned issues. These NCBMs have received considerable attention for stabilizing LMAs due to their unique structure, large specific surface areas, abundant surface groups, high mechanical strength, excellent thermal stability, and environmental friendliness. Considering the rapidly growing research enthusiasm for this topic in the last several years, here, we review the recent progress on the application of NCBMs in stable and dendrite-free LMAs. The different structures and modification methods of natural clays are first summarized. In addition, the relationship between their modification methods and nano/microstructures, as well as their impact on the electrochemical properties of LMAs are systematically discussed. Finally, the current challenges and opportunities for application of NCBMs in stable LMAs are also proposed to facilitate their further development.

1. Introduction

Nowadays, energy crisis and environmental pollution are significant issues facing the world [1]. The development of clean and sustainable energy, such as wind energy and solar energy, is crucial to solve the above-mentioned issues [2]. However, these clean and sustainable energy intrinsically have intermittent and fluctuation issues, leading to low energy utilization efficiency [3]. In this context, electrochemical energy storage devices are receiving wide attention in recent years due to their excellent adaptability, simple maintenance, and high energy-conversion efficiency [4]. Among them, lithium-ion batteries (LIBs) have been widely studied and commercialized due to their significant advantages, such as long lifespan, low self-discharge rate, and no memory effect [5]. Nevertheless, commercialized LIBs with limited practical energy density (100–220 Wh/kg) have been unable to satisfy the rapidly growing energy density demand, especially for long-range electric vehicles [6–8]. Hence, it is urgent to develop high-performance batteries with high energy density and long lifespan [9,10], which require high-capacity anode materials, cathode materials, as well as high-performance electrolytes and separators [11,12]. In this regard, lithium metal has been regarded as one of the most promising anodes because of their high theoretical specific capacity (3860 mAh/g) and low electrochemical potential (−3.04 V *vs.* standard hydrogen electrode) [13–15]. However, the practical application of lithium metals anodes (LMAs) still faces severe challenges, including uncontrollable dendritic growth, unstable solid electrolyte interface (SEI), resulting in low Coulombic efficiency and even serious safety hazards [13,16].

* Corresponding authors.
E-mail addresses: liuyong209@haust.edu.cn (Y. Liu), jjt0907@163.com (J. Ji), zhangqiaobao@xmu.edu.cn (Q. Zhang).

https://doi.org/10.1016/j.cclet.2024.109589
1001-8417/

To solve the aforementioned issues, various strategies have been explored, including introducing solid-state electrolytes (SSEs) [17,18], constructing artificial SEI on current collector surface [19], host design [20–22], liquid electrolytes optimization [23,24], advanced separator [25], and constructing SEIs on Li metal surface [26]. In recent years, natural clay-based materials (NCBMs) have attracted extensive attention for stabilizing LMAs because of their natural abundance, unique structures (mainly 1D and 2D structures), large specific surface area, rich charges distribution, abundant surface functional groups, high mechanical strength, and excellent thermal stability [27–29]. Specifically, NCBMs have unique structures which can provide lithium ion transport channels and regulate the uniform Li^+ deposition [30,31]. For example, Li *et al.* constructed an artificial SEI layer containing layered montmorillonite to achieve a high average Coulombic efficiency of 99.1% in Li/Cu half-cell over 400 cycles at 1 mA/cm^2 [30]. Furthermore, the NCBMs can interact with Li^+ due to their rich charge distribution, increasing the concentration of Li^+ on the surface of Li metal anode and promoting uniform lithium deposition [32,33]. For instance, Ma *et al.* developed an electrolyte containing vermiculite sheets (VS), with which the Li/$LiFePO_4$ full cells could exhibit a high specific discharge capacity of 137 mAh/g at 0.5 C, and a low fading rate of 0.034% per cycle over 150 cycles [32]. This excellent cycling performance could be ascribed that VS with negative charge can adsorb Li^+ and co-deposit on current collector, as well as their 2D structure and high modulus, leading to flattened Li nucleation and effectively suppressing the lithium dendritic growth [32]. Moreover, NCBMs possess high mechanical strength and excellent thermal stability, which can suppress the uncontrolled growth of Li dendrites and improve the safety of lithium metal batteries (LMBs) [34–36]. In addition, Lan *et al.* summarized recent advances of natural clay-based materials in the applications of energy storage and conversion, including Li-ion batteries, Li-S batteries, Zn-ion batteries, solar cells, and fuel cells [27]. Recently, Li and co-workers reviewed the application of natural clay minerals in Li-S batteries, especially in sulfur cathode hosts, separators, electrolyte and Li anodes [37]. Although a few reviews on Li anode of Li-S batteries have been published, nevertheless, to the best of our knowledge, the ones exclusively focusing on application of NCBMs in lithium metal anode for LMBs were rarely reported. Considering the rapidly growing research enthusiasm on this topic over the last several years, a timely and systematic review that covers the structure, modification methods and working principles of NCBMs in stable and dendrite-free LMAs is necessary.

In this review, we summarize the recent progress on the application of NCBMs in stable and dendrite-free LMAs. First, the classification, different structures, and modification strategies of natural clay materials are introduced, and the modification strategies are mainly including acidic treatments, ionic exchange, polymer-modified clay, and so on. Furthermore, the relationship between their modification methods and nano/microstructures, as well as their impact on the electrochemical properties of LMAs are systematically discussed. Finally, challenges and prospects for future development directions are proposed. We hope this review could be useful for designing and fabricating high-performance natural clay-based LMBs and boosting their practical applications.

2. Classification, structures, and modification strategies of natural clays

As a common type of natural silicate materials, natural clay materials consist of silica and alumina as their main components, as well as other oxides of magnesium, iron, calcium, sodium, and potassium in relatively small proportions in different clays [27]. In the structures of natural clays, $Si_2O_6(OH)_4$ units constitute tetrahedral silicon sheets, and $Al_2(OH)_6$ units constitute octahedral aluminum sheets [38]. These tetrahedral silicon sheets and octahedral aluminum sheets in the clays are bonded in a ratio of 1:1 (T-O) and 2:1 (T-O-T). According to different layered structures, nature clay minerals can be classified into four categories, including 1:1 type layer (kaolinite), 1:1 type tube (halloysite), 2:1 type layer (montmorillonite, vermiculite, illite *etc.*), 2:1 layer-chain type (attapulgite, sepiolite) and so on [29]. Furthermore, according to different dimensional structures, natural clays could also be divided into three types: one-dimensional (1D) clays, two-dimensional (2D) clays, and other types which are illustrated in Fig. 1.

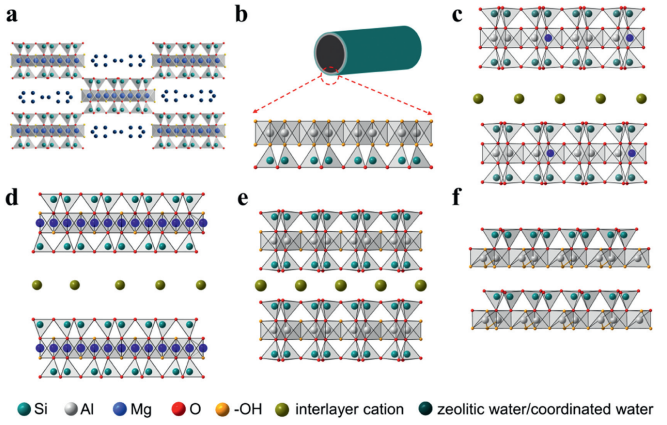

Fig. 1. Schematic illustration of different structures of various clay minerals: (a) Sepiolite, (b) halloysite, (c) montmorillonite, (d) vermiculite, (e) illite, (f) kaolinite.

2.1. Different structures of natural clay materials

2.1.1. 1D natural clay materials

The 1D natural clays mainly include attapulgite, sepiolite, and halloysite [27,29]. Attapulgite is also called palygorskite, which is a hydrated magnesium aluminum silicate mineral, and the general chemical formula of attapulgite is $(Mg, Al)_4(Si, Al)_8(O, OH, H_2O)_{26}\cdot nH_2O$ [39]. Attapulgite clay has a porous fibrous nanorod structure and the channels of attapulgite contain zeolite water and bound water. For attapulgite, Si is frequently substituted by Al, thus generating negative charges [40]. Owing to the excellent chemical stability, thermal stability, and strong adsorption capacity, attapulgite can enhance the mechanical strength and safety of its composites. Furthermore, sepiolite is a magnesium-rich fibrous porous clay mineral, and the standard crystal chemical formula is $Mg_8Si_{12}O_{30}(OH)_4(OH_2)_4\cdot 8H_2O$ [41]. The channels of sepiolite are filled with exchangeable cations, coordinated water molecules, and weakly bound zeolite water (Fig. 1a). Meanwhile, sepiolite plays an important role in adsorption application, which is related to the exchangeable cations and a high theoretical specific surface area. However, the hydrogen bonds between the fibers of sepiolite make it difficult to disperse uniformly, which limits the actual surface area of sepiolite [27]. In addition, halloysite has a unique multilayer nanotubular structure (Fig. 1b), and the general structural formula is $Al_2(OH)_4Si_2O_5\cdot H_2O$ [42]. Typically, halloysite nanotubes range in length from 0.02 μm to 30 μm, as well as their external diameters and inner diameters range from 30 nm to 190 nm and from 10 nm to 100 nm, respectively [43]. Due to the small contribution of the positive charges of the Al_2O_3 inner surface, the zeta potential of halloysite can be roughly described by the negative charges of the SiO_2 outer layer, which makes the halloysite nanotubes rich in negative charges [44]. Also, halloysite has excellent adsorption capacity because of its special tubular structure.

2.1.2. 2D natural clay materials

The 2D natural clays mainly include montmorillonite, vermiculite, and illite [27,29]. The chemical formula of montmorillonite is $(Na, Ca)_{0.33}(Al, Mg)_2(Si_4O_{10})(OH)_2{\cdot}nH_2O$ [29]. As shown in Fig. 1c, Montmorillonite has a layered structure, consisting of an alumina octahedral layer sandwiched between two silicate tetrahedral layers [45]. Among them, the Si and Al elements in the polyhedron are partially substituted by the low-valent Al and Mg elements to exhibit negative charges. Interlayer cations (Ca^{2+}, Na^{+}, Mg^{2+}, K^{+}, Fe^{2+}, *etc.*) are adsorbed in the interlayer to balance the excess negative charges. Due to the relatively weak bonding between the montmorillonite layers, interlayer cations could be exchanged with other cations. Meanwhile, the interlayer of montmorillonite will also allow liquid to enter, which will form fast ion transfer channels [30,46,47]. Moreover, the arrangement of polyhedral in vermiculite is similar to that of montmorillonite, and the structure of vermiculite is a layered magnesium aluminosilicate structure composed of an Mg-based octahedral sheet sandwiched between two tetrahedral silicate sheets (Fig. 1d). Vermiculite will expand several times in volume at high temperature, and expanded vermiculite possesses excellent ion exchange capacity and can be easily exfoliated into nanosheets [48,49]. In addition, the general structural formula of illite is $K_{1-1.5}Al_4[Si_{6.5-7}Al_{1-1.5}O_{20}](OH)_4$. Potassium ions between the illite layers form strong bonds (Fig. 1e), making illite difficult to exfoliate and cation exchange. Therefore, the adsorption capacity and cation exchange capacity of illite are not as high as montmorillonite [50].

2.1.3. Others

In addition to above-mentioned 1D and 2D natural clays, there are also other types of natural clays, such as kaolin and diatomite [27,37]. Kaolin belongs to the 1:1 type of clay consisting of silica tetrahedral nanosheets attached to alumina octahedral nanosheets (Fig. 1f). However, kaolin often exhibits different nanosheet or nanotube morphologies. Due to the strong hydrogen bonds between the layers and van der Waals forces, the structure of kaolin is stable and the interlayers are generally not easy to expand. Therefore, kaolin has excellent chemical and thermal stability [45]. Moreover, diatomite is derived from the remains of ancient diatoms and has two types: disk type and linear type. Amorphous silica is the main component of diatomite [51]. The porosity of diatomite is about 90%. Therefore, diatomite has the advantages of low density, large specific surface area, and strong adsorption capability [27,52]. In addition, the modification is necessary for avoiding the drawbacks of natural clays, such as limited specific surface area, unsatisfactory interlayer spacing and porosity. A series of modification methods have been applied for natural clays, including acid treatment [27], ion exchange modification [29], polymer modification [53], pillared clay [54], heat treatment [55], and mechanical treatment [56], which are systematically introduced and discussed in the following sections (Fig. 2).

2.2. Modification methods of natural clays

2.2.1. Ionic exchange

Due to the partial substitution of high-valent elements (Si, Al) in the clay by low-valent elements (Al, Mg) in the natural environment, the clay surface has excess negative charges. The negative charges on the clay surface and the coulomb electrostatic force of the cations provide favorable conditions for the ionic exchange of clay cations. At present, inorganic cations (Li^{+} [57], Co^{2+} [58], Zn^{2+} [59], Cu^{2+} [60], Fe^{3+} [61], *etc.*) have been used in the cation exchange modification strategies. Generally, after inorganic cation exchange, the interlayer spacing of clay will be changed with different interlayer cations [62]. Furthermore, the ionic exchange method also can change the number of layers of 2D clay,

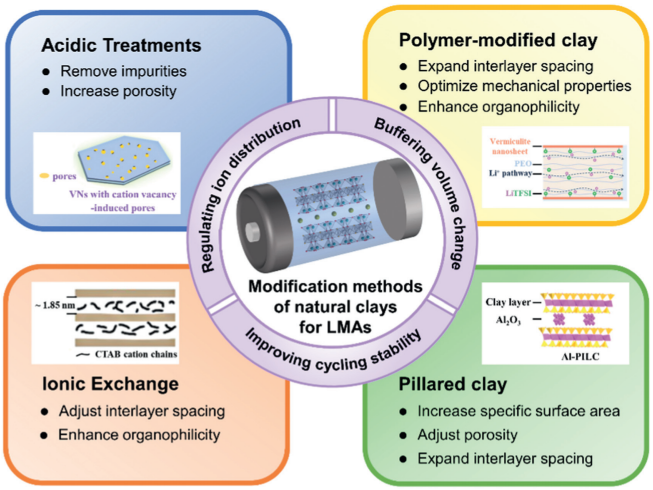

Fig. 2. Schematic diagram of the common used modification strategies of natural clays for lithium metal anodes.

such as preparing monolayer clay nanosheets [32,63,64]. For example, He *et al.* prepared monolayer vermiculite nanosheets *via* ionic exchange method and developed an ultrathin fire-proof framework (UFF) with a large specific surface area (137 m^2/g) by electrospinning and heating treatment [63]. Subsequently, this UFF was used to prepare composite solid electrolytes with a thickness of 4.2 μm. This composite solid electrolyte and achieve high Li^{+} conductivity of 2.1×10^{-4} S/cm at 25 °C due to the efficient transport pathways of Li^{+} between monolayer vermiculite nanosheets and polymers.

In addition to inorganic cations, the organic cations have also been utilized for ionic exchange modification, which not only enlarges the clay interlayer spacing but also converts the clays from hydrophilicity to hydrophobicity, thereby increasing the compatibility of the inorganic clay with the organic matrix [53]. During the organic cation exchange process, the cationic head groups of the polymer preferentially adsorb on the surface of the clay layer, while the cationic segments enlarge the clay interlayer spacing and convert the raw hydrophilic clay into a hydrophobic organoclay. For the composite polymer electrolytes in LMBs, the excellent compatibility between inorganic fillers and polymer matrix can significantly improve its Li^{+} conductivity due to the construction of uniform inorganic filler-polymer interface as Li^{+} transport pathway [28]. For instance, Park's group added quaternary ammonium salt modified organophilic MMT to polymer-based solid-state electrolyte, and the composite electrolyte exhibited a high Li^{+} conductivity of 1.6×10^{-3} S/cm at 25 °C [46].

2.2.2. Acidic treatments

Acid treatment is a commonly used strategy for the purification and performance enhancement of natural clays [53,56]. On one hand, in the natural environment, the raw clays contain many impurities, including metal oxides, carbonates, quartz, *etc.* As an important process for clay purification, acid treatment can remove most of metal oxide impurities [65]. On the other hand, acid treatment could partially dissolve Mg and Al atoms from the crystal lattice, and increase the specific surface area and porosity of clays [66]. For example, Li *et al.* developed a large number of cationic vacancies on 2D vermiculite nanosheets by acid treatment and used them as filler, which greatly improved the Li^{+} conductivity (2.6×10^{-3} S/cm at 27 °C) and electrochemical stability (4.9 V) of polymer-based solid electrolytes [31]. This high Li^{+} conductivity could be ascribed that the acid treatment could remove Mg and Al atoms in vermiculite, enhancing the Lewis acid-base interaction between vermiculite and Li^{+} and promoting Li^{+} transport. Notably,

the effect of acid treatment is related to many factors, including acid type, chemical composition of clays, as well as time and temperature of treatment, which should be adjusted according to the requirements of clay application [67].

2.2.3. Polymer-modified clay

Natural clays such as montmorillonite possess strong hydrophilicity, which leads to uneven distribution of clay within the polymer matrix, thereby limiting the mechanical properties, thermal stability, and Li^+ conductivity of clay-polymer composites. The dispersion of natural clays in polymer matrices could be optimized by introducing different polymers into interlayer of natural clays *via* physical adsorption and chemical grafting [68]. To date, polyvinyl alcohol (PVA), polyacrylamide (PAM), polyvinyl chloride (PVC), polyurethane (PU), polypropylene (PP), chitosan, and polystyrene (PS) have been added into interlayer of natural clays, forming polymer-clay composites [69,70]. Among these polymer-clay composites, there is an interaction between polar polymers and natural clays, such as PVA and MMT, which can significantly enhance the thermal stability and mechanical properties of clay-polymer composites [71]. In addition, the immiscibility of clays with non-polar polymers (PP, PS, *etc.*) can be solved by organoclay modification methods. For composite electrolytes in LMBs, the excellent wettability between polymer-modified clay and polymer electrolyte can improve the dispersion of inorganic clay in the organic matrix, endowing high Li^+ conductivity of composite electrolytes. For example, after modificated by D-α-tocopherol-polyethylene glycol 1000 succinate, sepiolite can be uniformly dispersed in PEO electrolyte, and the composite electrolyte exhibited a high Li^+ conductivity of 5×10^{-4} S/cm at 25 °C [72].

2.2.4. Other methods

In addition to aforementioned modification strategies, pillared clay, heat treatment and mechanical modifications are also used for natural clay modification [29,56]. Pillared clay is an important natural clay modification method, and the introduction of metal compounds (Al_2O_3 [54], TiO_2 [73], CeO_2 [74], CoS_2 [58], *etc.*) into clay interlayers could not only increase the specific surface area and adjust the porosity of clays, but also endow the clay materials with high adsorption and catalytic performance [75]. Furthermore, heat treatment also can significantly change the porosity and specific surface area of the natural clays, and the optimum treatment temperature varied with different clay materials, which is associated with the clays' compositions and structures [29,76]. In addition, mechanical modifications, such as grinding, also can change the shape and size of the clays [77].

As discussed in Sections 2.2.1–2.2.4, various modification methods of natural clays can change their structure and thereby improve their properties. Ionic exchange can change the interlayer spacing and hydrophilic properties of natural clays. Furthermore, acid treatment could not only significantly change their structures but also adjust their compositions. Moreover, polymer modification can convert the natural clay from hydrophilicity to hydrophobicity. In addition, pillared clay can adjust the porosity, and increase the interlayer spacing and specific surface area of natural clays. The properties of NCBMs are closely related to their structure, such as interlayer spacing, specific surface area, and porosity. At the same time, the properties of NCBMs also depend on their composition. Therefore, to obtain the NCBMs with desired properties, a combination of various modification methods is often used.

3. Application of NCBMs in stable LMAs

NCBMs have unique structures and charge distribution, which are conducive to achieving fast and uniform Li^+ transport [28]. In addition, NCBMs also have significant advantages of low cost and environmental friendliness. Hence, many strategies with NCBMs have been investigated for stabilizing LMAs, including introducing solid state electrolytes [31,44,48,49,54,57,65,72,78–91], constructing artificial SEI on current collector surface [30,92,93], host design [94], liquid electrolyte optimization [32,95], and other strategies [34–36,96–99]. More details about the electrochemical performance could be found in Table 1.

3.1. Introducing solid-state electrolytes

In liquid electrolyte LMBs, side reactions will continuously occur between LMAs and liquid electrolyte during cycling, resulting in a low Coulombic efficiency and uncontrollable lithium dendrite growth [100]. In this context, introducing solid-state electrolytes to replace liquid electrolytes can effectively avoid aforementioned side reactions and thereby improve the electrochemical performance and safety of LMBs [28]. Compared to inorganic solid-state electrolytes, solid polymer electrolytes (SPEs) have good physical contact with LMAs due to their excellent flexibility, leading to low interfacial resistance [101]. However, at room temperature, SPEs still suffer from unsatisfactory ionic conductivity, inferior Li^+ transference number, weak mechanical strength, and narrow electrochemical window, which hinder their practical applications [102]. In this regard, NCBMs have been used as fillers to SPEs to improve electrochemical and mechanical properties of SPEs. In recent years, various composite polymer electrolyte based on NCBMs have been fabricated through *ex-situ* solidification method and *in-situ* solidification technique, which have received considerable attention [48,49,65,82,86].

Ex-situ solidification method, such as solution casting method, is a promising method for large-scale fabrication of SPE [103]. So far, various types of NCBMs were added in polymer electrolyte *via ex-situ* solidification method, and the composite SSEs achieved improved ionic conductivity, Li^+ transference number, mechanical strength, and thermal stability [31,44,48,49,54,57,65,72,78–87,89,90]. For example, Tang *et al.* developed a composite solid electrolyte consisting of PEO and vermiculite sheets (VS) *via* solution-casting method [49]. Results showed that the highly active interface between PEO and VS reduced the crystallinity of the PEO and improved the ionic conductivity to 2.9×10^{-5} S/cm at 25 °C). Moreover, the VS enhanced composite electrolyte exhibits wide electrochemical operation window (about 5.35 V *vs.* Li/Li^+) under 25 °C and dimensional stability at 200 °C, which can ensure the safe and stable LMBs. Furthermore, Tang *et al.* introduced vertically aligned vermiculite sheets (VAVS) to PEO electrolyte to prepare a composite electrolyte (PEO/VAVS) through a directional freezing method followed by vacuum infiltration [48]. Compared to the composite electrolyte with disordered distribution of VS, the composite electrolyte with VAVS provided continuous Li^+ transport pathways through the composite electrolyte, which could exhibit excellent ionic conductivity (1.89×10^{-4} S/cm at 25 °C). Meanwhile, the nanoindentation test result indicated that this composite electrolyte with VAVS exhibited a high modulus of 44.5 MPa, which could effectively prevent short circuit between cathodes and LMAs. In addition, Lv *et al.* prepared a nano-dipole doped composite polymer electrolyte (NDCPE) containing dipole-like halloysite nanotubes (d-HNTs) *via* solution casting technique [86]. As shown in Fig. 3a, the d-HNTs had negative charges on the outer surface and positive charges on the inner surface, promoting the dissociation of lithium salts. Consequently, the unique charge distribution of d-HNTs not only facilitated the rapid transport of Li^+-solvent complex, but also can effectively adsorb anions, effectively improving the Li^+ conductivity (2.9×10^{-4} S/cm), Li^+ transference number (0.75), and electrochemical window (5 V) at room temperature. Moreover, the D-HNTs could induce the formation of β-PVDF, which inhibited the space charge region on

Table 1
The electrochemical performance of NCBMs for stable LMAs.

Materials	Clay utilized	Ionic conductivity (S/cm)	Reversible capacity (DC[a], CD[b])	Cycling stability (DC, CD, CN[c])	Refs.
Introducing solid state electrolytes					
VNs	Vermiculite	2.6×10^{-3} at 27 °C	152.2, 0.2 C	140.2, 0.2 C, 500	[31]
Halloysite nanotubes	Halloysite	9.23×10^{-5} at 25 °C	171.6, 0.1 C	156, 0.1 C, 100	[44]
VAVS	Vermiculite	1.89×10^{-4} at 25 °C	167, 0.1 C	~137, 0.5 C, 200	[48]
VS	Vermiculite	2.9×10^{-5} at 25 °C	152, 0.5 C	–	[49]
Al-pillared clay	Montmorillonite	2.13×10^{-3} at 25 °C	111, 0.5 C	120, 0.5 C/, 1000	[54]
Li-MMT	Montmorillonite	0.48×10^{-3} at 25 °C	5.76 mAh, 0.1 mA/cm^2	5.11 mAh, 0.1 mA/cm^2, 200	[57]
UFF	vermiculite	2.1×10^{-4} at 25 °C	177, ~7 C	138, ~7 C, 100	[63]
Organophilic MMT	Montmorillonite	1.6×10^{-3} at 25 °C	152, 0.2 C	135, 0.5 C, 200	[65]
TPGS-S@TPE	Sepiolite	0.5 at 25 °C	~140, 0.5 C	~120, 0.5 C, 100	[72]
TPGS-S@PEO	Sepiolite	7.8×10^{-4} at 30 °C	142, 0.05 C	110, 0.05 C, 30	[78]
Palygorskite nanowires	Palygorskite	1.2×10^{-4} at RT	117.6, 0.3 C	118.1, 0.3 C, 200	[79]
Li-MNT	Montmorillonite	3.5×10^{-4} at 25 °C	145.9, 0.5 C	~134.1, 0.5 C, 200	[80]
Halloysite nanotubes	Halloysite	5.62×10^{-5} at RT	138.3, 0.2 C	117.4, 0.2 C, 150	[81]
MMT nanosheets	Montmorillonite	1.06×10^{-3} at RT	140, 0.3 C	>137.2, 0.3 C, 400	[82]
VAMMT	Montmorillonite	1.08×10^{-3} at RT	137, 0.5 C	~118, 0.5 C, 1000	[83]
2D Ht	Montmorillonite	1.08×10^{-4} at 30 °C	148.7, 0.2 C	134, 0.2 C, 100	[84]
Li-MMT@PPL122	Montmorillonite	1.82×10^{-3} at 25 °C	162.5, 0.2 C	120, 1 C, 1000	[85]
d-HNTs	Halloysite	2.9×10^{-4} at RT	136, 1 C	118.4, 1 C, 300	[86]
Li-MMT@VA-CSE	Montmorillonite	1.99×10^{-3} at RT	144, 0.5 C	149.6, 0.5 C, 200	[87]
Vr-NH_2	vermiculite	1.35×10^{-3} at 100 °C	158.6, 0.2 C	152.3, 0.2C, 200	[88]
OMMT	Montmorillonite	1.1×10^{-3} at RT	138.8, 0.5 C	147.4, 0.5 C, 100	[89]
Halloysite nanotubes	Halloysite	1.23×10^{-3} at RT	150, 0.5 C	118, 0.5 C, 1000	[90]
Kao-DMSO	Kaolin	8.58×10^{-4} at 25 °C	140.5, 0.5C	113.8, 0.5 C, 800	[91]
Constructing SEIs on current collector surface					
Li-MMT	Montmorillonite	–	120, 1 C	~108, 1 C, 400	[30]
Ag-MMT	Montmorillonite	–	111.2, 5 C	116.7, 1 C, 500	[93]
Host design					
Silicide-Li composite	Diatomite	–	~148, 0.5 C	117, 0.5 C, 500	[94]
Liquid electrolytes optimization					
Vermiculite sheets	Vermiculite	–	~135, 0.5 C	130.4, 0.5 C, 150	[32]
Montmorillonite	Montmorillonite	–	–	–	[95]
Advanced separators					
Talcum	Talcum	5.09×10^{-4} at 25 °C	145.9, 0.5 C	122.6, 0.5 C, 400	[35]
ASN	Vermiculite	1.14×10^{-4} at 30 °C	161, 1 C	139.7, 1 C, 1000	[36]
Li-MMT@PP in DOL/DME/LiTFSI	Montmorillonite	–	–	–	[96]
Vermiculite sheets/PVDF/PAN	Vermiculite	1.02×10^{-3} at 20 °C	156, 2 C	155.8, 2 C, 200	[97]
Li-MMT@PP in DME/LiFSI	Montmorillonite		142.7, 1 C	142.3, 1 C, 200	[99]
Constructing artificial SEI on Li metal surface					
Li-HNTs	Halloysite	–	115, 2 C	~112, 2 C, 800	[34]
Vermiculite sheets	Vermiculite	–	2 mAh/cm^2, 0.4 C	1.6 mAh/cm^2, 0.4 C, 140	[98]

[a] DC: Discharge capacity (mAh/g).
[b] CD: Current density.
[c] CN: Cycle number.

the LMA surface and formed a stable LiF-enrich SEI (Fig. 3b). As a result, the Li/Li cells with NDCPE displayed an excellent rate performance even at a current density of 1 mA/cm^2 (Fig. 3c). The above excellent electrochemical performance are attributed to that d-HNTs could promote the dissociation of lithium salts and provide a Li^+-transport friendly microenvironment [86].

In addition to *ex-situ* formed SPEs, the preparation of composite solid electrolytes by *in-situ* solidification technology can simultaneously improve the interface contact between the electrolyte and the cathodes/LMAs, exhibiting low interface impedance [104,105]. To date, a series of NCBMs have been fabricated for stable LMAs *via in-situ* solidification technology [65,81]. For instance, Young *et al.* prepared PVDF-HFP/MMT nanosheets composite polymer-clay electrolytes (U-CPCE) using *in-situ* ultraviolet (UV) crosslinking method [65]. Compared to UV-crosslinked gel polymer electrolyte (U-GPE) electrolyte, U-CPCE exhibited an excellent ionic conductivity (up to 1.6×10^{-3} S/cm at 25 °C) due to the increasement of amorphous region of PVDF-HFP. Meanwhile, benefiting from the addition of MMT, U-CPCE exhibited high electrochemical window of 5 V, ensuring high safety and cycling stability of LMBs. More interestingly, the MMT with a high dielectric constant promoted the dissociation of lithium salt and interacted with polymer chains, which not only weakened the interaction between Li^+ and polymer chains but also restricted the migration of large-sized anions, and thereby improved Li^+ transference number from 0.52 to 0.78 (Fig. 3d). Therefore, when combined with $LiCoO_2$ cathode, the full cell with U-CPCE exhibited high capacity retention under 0.5 C after 200 cycles (from 141 mAh/g to 135 mAh/g, 96%) and excellent rate capability (Figs. 3e and f). These excellent electrochemical performance can be attributed to the synergistic effect of interaction between high dielectric constant MMT and PVDF-HFP matrix [65]. Moreover, Wang *et al.* fabricated a solid composite electrolyte

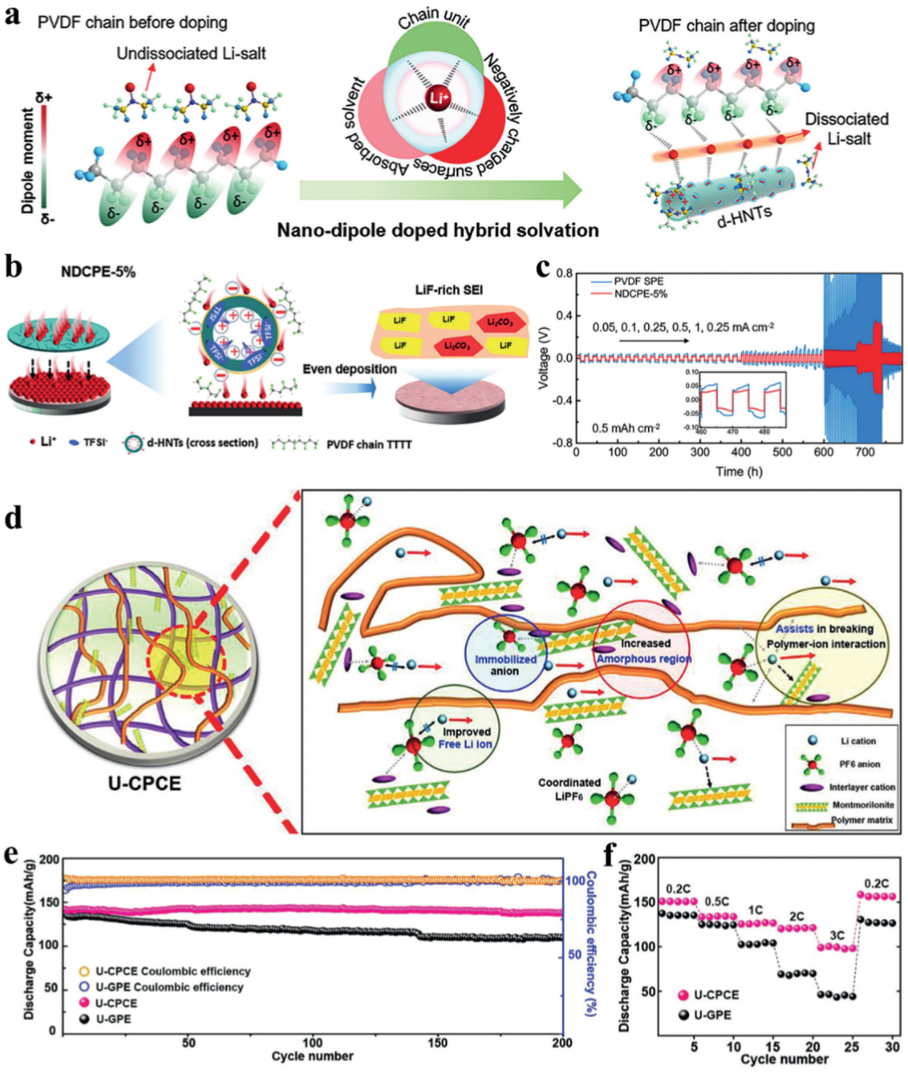

Fig. 3. (a) Schematic illustration of the mechanism for d-HNTs enhanced Li^+ transport performance. (b) Mechanism diagram of d-HNTs suppression of space charge region and construction of stable SEI. (c) Comparison of rate performance of Li/Li cells with NDCPE and PVDF SPE at different current density. (d) Schematic illustration of the ionic transport mechanism and the factors affecting the improvement of ionic conductivity. (e) Discharge capacity and coulombic efficiency during cycles at 0.5 C charge/discharge and (f) Rate performances of the Li/$LiCoO_2$ cells with U-CPCE and U-GPE under different C-rates. (a-c) Adapted with permission [86]. Copyright 2023, Elsevier B.V. (d-f) Adapted with permission [48]. Copyright 2019, Wiley-VCH. (g-i) Adapted with permission [65]. Copyright 2020, Wiley-VCH.

(CMP/MMT) by *in-situ* UV cross-linked method, which exhibited good thermal stability in flammability test and excellent ionic conductivity of ~1.06 mS/cm at room temperature [82].

The electrochemical performance of polymer SSEs could be enhanced by introducing NCBMs as fillers. Based on the above studies, some common features could be found in these NCBMs containing composite SSEs: (1) NCBMs have a large specific surface area, which can significantly reduce the crystallinity of the polymer matrix and improve ionic conductivity; (2) NCBMs can provide Li^+ transport channels to improve Li^+ conductivity; (3) NCBMs can promote the dissociation of lithium salts and improve the Li^+ transference number; (4) NCBMs have excellent mechanical strength and inhibit Li dendrite growth; (5) NCBMs have good thermal stability, thereby improving the safety of LMBs.

3.2. Constructing artificial SEI on current collector surface

The current collectors (such as copper foil, copper mesh, carbon cloth) significantly affect the Li deposition behavior. During charging process in LMBs, Li^+ tends to deposit on uneven hot spots of current collector, especially for planar current collector, resulting in Li dendrite growth [106]. In this context, NCBMs are used to prepare artificial SEI layers on current collector surface to relieve Li dendrite due to their good Li^+ conductivity and high mechanical strength for stable LMAs [30,92,93]. For instance, Nan *et al.* prepared Li-MMT to construct an artificial SEI on copper foil *via* blade coating method [30]. In this artificial SEI, Li-MMT showed high mechanical properties and provided Li^+ transport channel to inhibit lithium dendrite growth. As shown in Fig. 4a, the results of finite element simulation prove uniform Li^+ concentration distribution on the surface of copper foil in Li-MMT SEI. On the contrary, the surface of bare copper foil exhibits significant concentration polarization, which would cause uncontrolled growth of lithium dendrites. As a result, the Li/Cu cell with Li-MMT SEI displayed a high specific capacity of 120 mAh/g and maintained high capacity retention of 90% after 400 cycles at 1 C (Fig. 4b). This excellent cycling stability could be ascribed that the Li-MMT can offer high mechanical strength and provide fast interlayer channels for Li^+ transport [30].

Although artificial SEIs containing NCBMs have high mechanical properties and abundant Li^+ transport channels, dendrite growth is inevitable at high current density due to uneven lithium nucleation

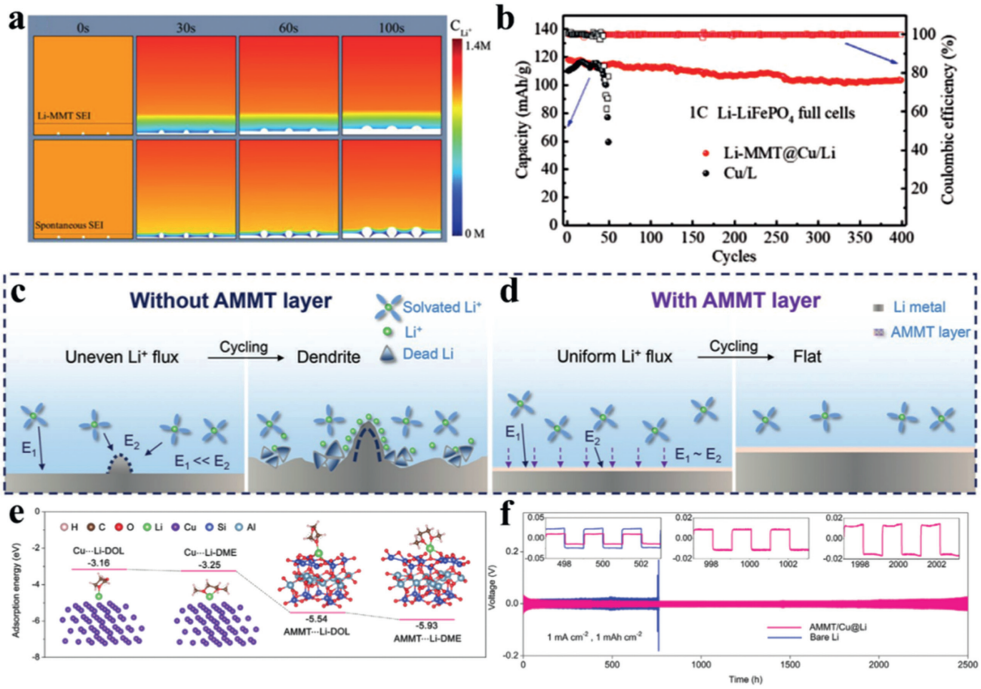

Fig. 4. (a) Finite element modeling of Li^+ concentration profiles and Li metal deposition on Li-MMT@Cu and Cu at 10 mA/cm^2. (b) The cycling performance of Li/$LiFePO_4$ full cells at 1 C. (c) Schematic diagram of deposition behavior and corresponding mechanisms of the undecorated anode. (d) Schematic diagram of deposition behavior and corresponding mechanisms of AMMT-modified anode. (e) Adsorption energies between solvent-coordinated Li and different substrates. (f) Voltage profiles at a current density of 1 mA/cm^2 with 1 mAh/cm^2. Insets: Voltage profiles at different stages. (a, b) Adapted with permission [30]. Copyright 2021, Wiley-VCH. (c-f) Adapted with permission [93]. Copyright 2023, Wiley-VCH.

and high nucleation barrier [106]. In this context, the strategies of introducing lithiophilic sites (*e.g.*, Ag, Sn, Bi) are widely studied, because adequate lithiophilic sites can serve as the lithium nucleation seeds to reduce nucleation barriers and guide the uniform Li deposition. The strategies of *in-situ* generating lithiophilic sites have also been applied to NCBMs-containing artificial SEIs for stable LMAs [93,107,108]. For instance, Zhang's group constructed an artificial SEI with Ag-montmorillonite (AMMT) on copper foil [93]. The lithiophilic Ag can be *in situ* formed in this artificial SEI during cycling, and the reaction equation is as follows:

$$xLi + yAg^+ + ye^- \rightarrow Li_xAg_y \quad (1)$$

The *in situ* formed Ag could reduce the Li^+ deposition energy barrier and guide uniform lithium deposition. Meanwhile, AMMT possessed layered Li^+ transport channels and negative charges, which could induce uniform Li^+ flux and achieve uniform lithium deposition (Figs. 4c and d). Furthermore, DFT calculation results showed that AMMT could reduce the solvation energy and accelerate the desolvation process of Li^+ (Fig. 4e). Consequently, Li/Li symmetric cells with AMMT displayed a lower overpotential (27 mV) under 1.0 mA/cm^2 and excellent cycling stability over 2500 h (Fig. 4f). These excellent electrochemical properties could be ascribed that the *in-situ* derived lithiophilic Li-Ag alloy is beneficial to uniform lithium deposition, and the AMMT could facilitate rapid Li^+ desolvation process [93].

3.3. Host design

Compared to "hostless" LMAs, host design can reduce local current density to achieve uniform lithium deposition and accommodate the Li metal's volume expansion during cycling [15]. In this regard, NCBMs is considered as a promising candidate for advanced lithium hosts due to their unique microstructure and high porosity [94,109,110]. For example, Zhou *et al.* prepared diatomite framework derived silicon (DF-Si) powder by magnesium thermal reduction, and the DF-Si powder was mixed with molten Li and coated by PEO-SPE to prepare a composite anode (PEO-DLSL) by cold pressing (Fig. 5a) [94]. As shown in Fig. 5b, lithium filled the pores of diatomite-derived composite anode, which achieved intimate contact between the electrode and the solid-state electrolyte. The simulation results of lithiation process of DF-Si framework show that porous structure is favourable for homogeneous Li^+ flux and fast Li^+ transport in composite anodes (Fig. 5c). Therefore, Li symmetric batteries exhibited a stable cycling performance for 1000 h at a current density of 0.5 mA/cm^2 (Fig. 5d). In addition, the Li/LFP all solid-state cells could also show a high specific discharge capacity of 65 mAh/g at 5 C (Fig. 5e). The excellent electrochemical performance could be ascribed that the unique three-dimensional structure of PEO-DLSL could reduce the local current density, which was conducive to uniform lithium plating and stripping even under high current density [94].

3.4. Liquid electrolyte optimization

In liquid electrolytes (LEs), improving the Li^+ concentration of LMA surface can alleviate the concentration polarization and suppress dendrites growth [33,111]. Due to their negative charges, NCBMs in LE can achieve high Li^+ concentration and promote uniform lithium deposition [32,95]. For instance, Ma *et al.* introduced vermiculite sheets (VS) into liquid electrolyte [32]. In the VS added liquid electrolyte, vermiculite sheets with negative charges could adsorb a large amount of Li^+, thereby forming the rock-like lithium-vermiculite composite. Due to the synergistic effect of the high mechanical modulus of vermiculite sheets and the high Li^+ concentration on the LMAs surface, the Li/Li symmetric cell with VS-containing electrolyte showed a good cycling stability over 600 h at a current density of 1 mA/cm^2 [32]. Further, Chen *et al.* developed a novel ether-based electrolyte containing montmorillonite implanted in PEO as an additive (MIP-based electrolyte), in which small amounts of PEO and montmorillonite were added

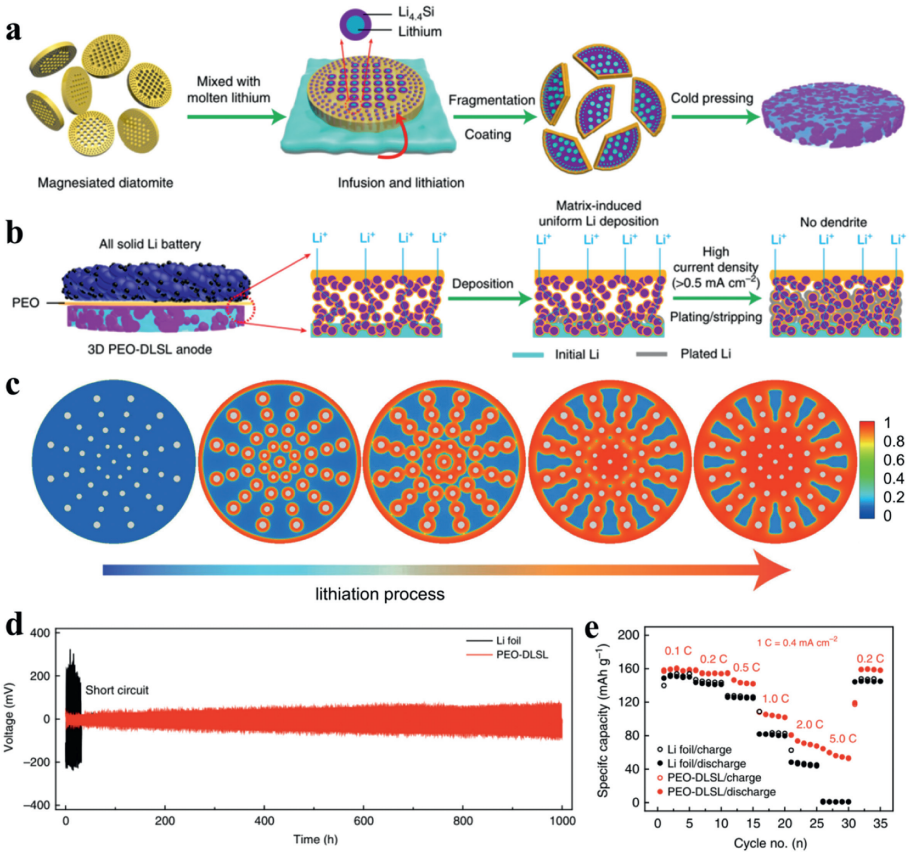

Fig. 5. The preparation, action mechanism, and electrochemical performance of DF-Si framework. (a) The fabrication process of PEO-DLSL. (b) Schematic diagram of lithium stripping/plating behavior in all-solid-state LMBs with PEO-DLSL anode. (c) The simulation of Li^+ diffusion into the DF-Si framework with the lithiation process. During the lithiation process, the variation from the blue color to red color represents the increase of Li concentration and lithiation extent of DF-Si. (d) Long-term cycling stability test of the Li/Li cells with PEO-DLSL and Li-foil anodes at a current density of 0.5 mA/cm^2. (e) The discharge capacity with different C-rates of Li/LFP full cells with PEO-DLSL and Li-foil anode. Adapted with permission [94]. Copyright 2019, The Author(s).

[95]. Compared with pure ether-based electrolytes, the Li^+ concentration on the surface of LMA is higher in MIP-based electrolyte, which could effectively delays the Sand's time and favorable for uniform lithium nucleation (Figs. 6a and b). *In-situ* Raman spectroscopy and optical microscope tests demonstrated the uniform lithium deposition behavior in MIP-based electrolyte (Figs. 6c and d). Therefore, the Li/Cu cells with MIP-based electrolyte could depict a stable and high platting/stripping capacity even at high current density of 4 mA/cm^2 and a high coulombic efficiency of 98.3% at 0.5 mA/cm^2 (Figs. 6e and f). Moreover, the Li/Li symmetrical cells with MIP-based electrolyte exhibited a excellent cycling performance at a current density of 1.0 mA/cm^2 and a low over potential of 10 mV (Fig. 6g). These excellent electrochemical performances can be attributed to the interaction between MMT and Li^+, as well as the optimized Li ion distribution in the MIP-based electrolyte [95].

3.5. Others

In addition to aforementioned strategies, other strategies have also introduced NCBMs to achieve stable LMAs, including advanced separators and constructing SEIs on current collector surface [19,112]. For the LMBs, the characteristics of separators significantly affect the rate capability, cyclic and safety performance, such as wettability, heat shrinkage resistance and mechanical strength [113]. However, due to the uneven distribution of pores, severe deformation under elevated temperature, and weak mechanical strength, the commercial separators are difficult to inhibit dendrite growth and avoid local thermal runaway [36]. Under this background, NCBMs can play an important role in improving the mechanical strength, thermal stability of the separators, and guiding homogeneous Li^+ flux for stable LMAs [35,36,96,97]. For example, Yang *et al.* developed an advanced separator with montmorillonite (Li-MMT@PP) to guide the uniform Li^+ flux by constructing Li^+ channels (Fig. 7a) [96]. Therefore, Li/Li symmetrical cells with Li-MMT@PP exhibited a uniform Li deposition behavior at a current density of 5 mA/cm^2 (Fig. 7b). Recently, Guo *et al.* prepared a low-cost inorganic separator, which is vermiculite-derived two-dimensional porous amorphous silica nanosheets (ASN-Sep) [36]. As shown in Figs. 7c-f, compared to commercial separators, ASN-Sep exhibited higher average Young's modulus (625 MPa), higher thermal resistance, and better electrolyte wettability, which endow the safety performance of LMBs. As a result, Li/Li cells with ASN-Sep depicted a low overpotential of 31 mV and stable cycling performance for 1500 h (Fig. 7g). These superior performance could be attributed to a large number of pores and abundant surface oxygen groups in ASN, which guided the even Li^+ flux, improving the Li^+ transference number and ionic conductivity [36]. Moreover, the strategies of constructing a robust artificial SEI by utilizing NCBMs on Li metal surface have also studied to improve the performance of LMA [34,98]. For example, Liu *et al.* prepared a nano composite layer (NCL) on Li metal with lithium-halloysite and PEO-based cross-linked network polymer as a new artificial SEI [34]. The NCL exhibited an appropriated mechanical strength, which could inhibit the dendritic growth and accommodate the volume change of LMAs during cycling. As a result, the Li/Li symmetric cells with NCL depicted stable cycling performance (over 1100 h at a current density of 1 mA/cm^2).

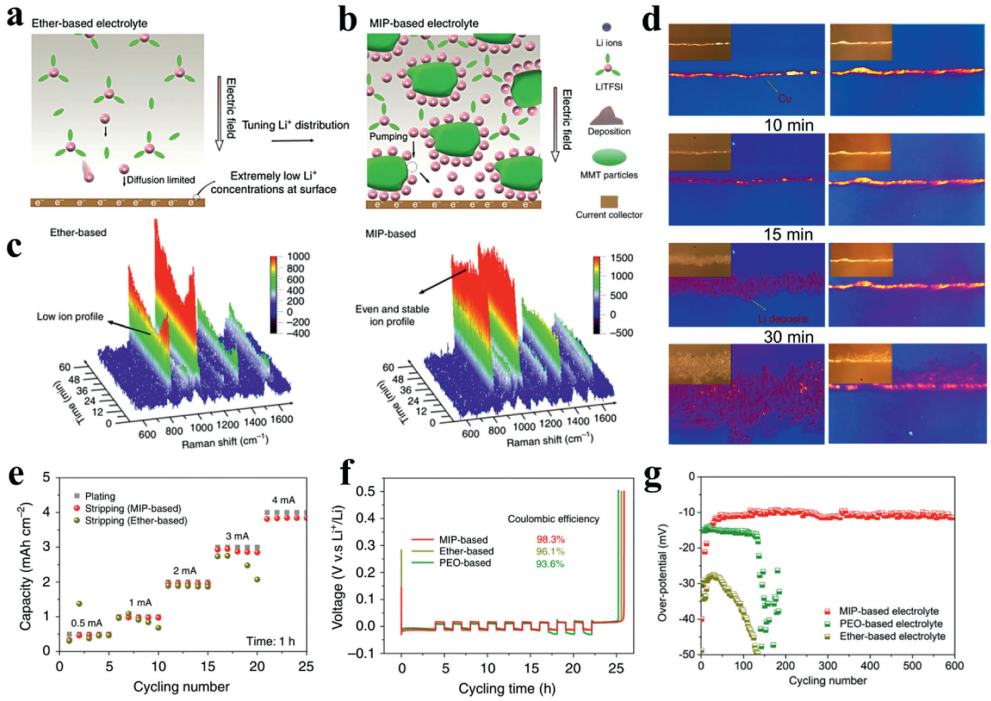

Fig. 6. The action mechanism and electrochemical performance of MIP-based electrolyte for stable LMAs. Schematic diagram of Li^+ transport and deposition behavior mechanism with (a) ether-based electrolyte and (b) MIP-based electrolyte. (c) *In situ* Raman spectra of ether-based electrolyte and MIP-based electrolyte, respectively. (d) Comparison of lithium deposition morphology in ether-based electrolyte (left column) and MIP-based electrolyte (right column) at 0, 10, 15, and 30 min at a current density of 3 mA/cm^2. (e) The rate capacity of lithium plating/stripping at different current density at one hour with different electrolytes. (f) Voltage-time curves of Li/Cu cells at 0.5 mA/cm^2 and the average Coulombic efficiency with different electrolytes. (g) The over-potential of Li/Li symmetric cells at 1 mA/cm^2 for different cycles. Adapted with permission [95]. Copyright 2019, the author(s).

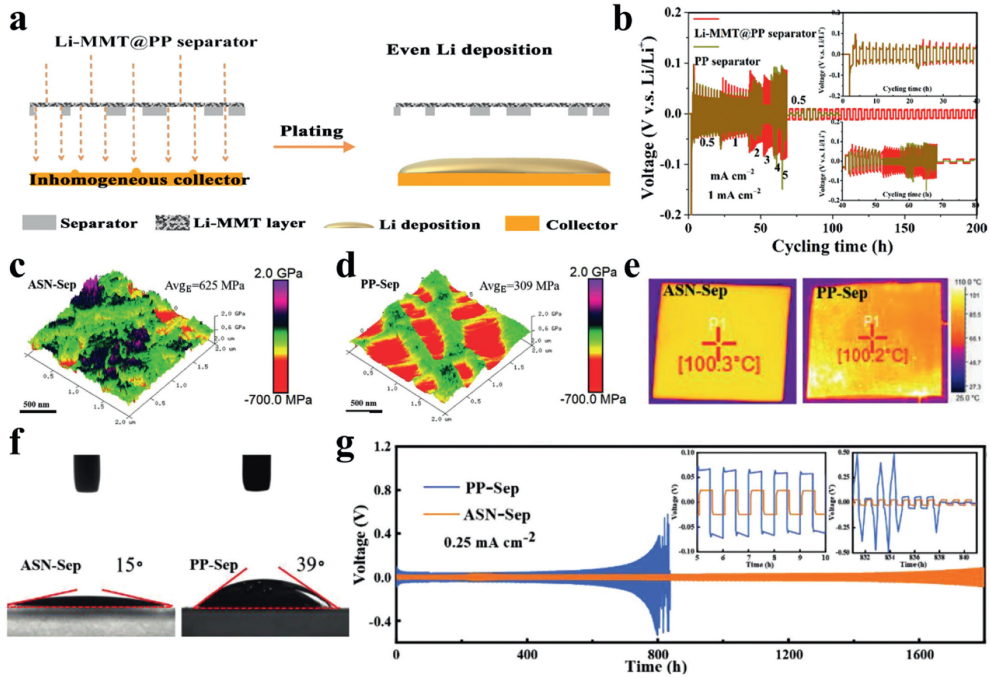

Fig. 7. (a) Schematics of design concepts with different Li-MMT@PP separator and PP separator. (b)The rate performances of Li/Li symmetric cells. Young's modulus of the as-prepared (c) ASN-Sep and the commercial (d) PP-Sep. (e) Thermal stability test of ASN-Sep and PP-Sep. (f) The electrolyte infiltration photos of ASN-Sep and PP-Sep. (g) Long-term cycling stability test of Li/Li symmetric cells with the PP-Sep and ASN-Sep at 0.25 mA/cm^2. (a, b) Adapted with permission [96]. Copyright 2021, the Author(s). (c-g) Adapted with permission [36]. Copyright 2023, Wiley-VCH.

3.6. Summary

As discussed in Sections 3.1–3.5, the applications of NCBMs for stable LMAs have been summarized, including introducing solid state electrolytes, constructing artificial SEI on Li metal surface, host design, liquid electrolyte optimization, and other strategies. Among these different strategies, introducing solid state electrolytes with NCBMs for stable LMAs is one of the most widely used strategies, which can greatly enhance the electrochemical performance and safety of LMBs. Compare to *ex-situ* solidification method, *in-situ* solidified composite SPEs with NCBMs could exhibit great cycling stability, due to the superior Li^+ transport performance at the compact electrolyte-electrode interface [65]. Furthermore, the artificial SEIs containing NCBMs exhibit increased mechanical strength and excellent Li^+ conductivity, which can inhibit Li dendrite growth during cycling. Moreover, benefiting from the interaction between NCBMs and Li^+, NCBMs can be used as electrolyte additives to achieve uniform Li^+ distribution in liquid electrolytes. In addition, the advanced separators with NCBMs could exhibit high mechanical strength and thermal stability, thereby significantly improving the safety performance of LMBs. At present, although great progress has been made on the research of NCBMs for stable LMAs, more attention should be paid to their practical applications.

4. Conclusions and outlook

In conclusion, we summarize recent progress on the applications of NCBMs for stable LMAs, including introducing solid-state electrolytes, constructing artificial SEI on current collector surface, host design, liquid electrolytes optimization, advanced separators, and constructing artificial SEI on Li metal surface. The classification, structures, and modification methods of natural clays are firstly summarized. The modification methods of natural clays include ionic exchange, acid treatment, polymer modification, pillared clay, thermal treatment, and mechanical treatment. Among them, the ionic exchange method is the most commonly used strategy. Furthermore, the utilization of NCBMs in stabilizing LMAs, and the relationship between synthetic methods, nano/microstructures, and electrochemical performance of natural clay-based LMAs are systematically discussed. NCBMs have many advantages for stabilizing LMAs, attributing to the following pivotal points: first, due to their large specific surface area and Li^+ transport channels, NCBMs can achieve rapid and even Li^+ transport. Second, NCBMs can also play an important role in inhibiting dendrite growth due to their high mechanical strength. Moreover, the unique charge distribution of NCBMs is conducive to the dissociation of lithium salts and the migration of Li^+. In addition, benefiting from their excellent thermal stability, NCBMs can significantly improve the safety properties of LMBs during cycling. Although some significant progress has been made on natural clay-based LMBs, many challenges remain to be solved, and researchers should pay more attention to the following aspects to boost their practical application (Fig. 8):

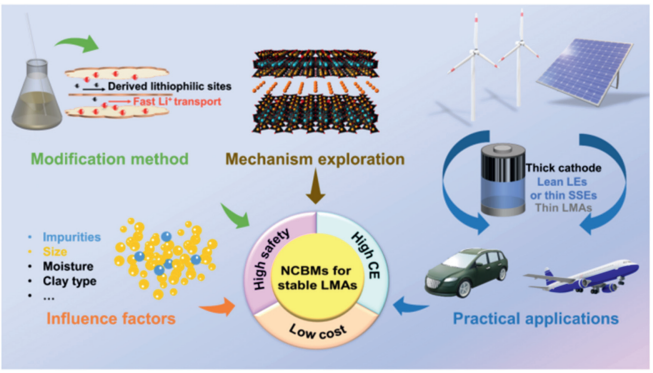

Fig. 8. Schematic illustration of future directions of NCBMs for stable LMAs.

(1) Influence factors. To further improve the electrochemical performance of natural clay-based LMBs, there are some important influence factors which should be paid attention to, such as impurity, particle size, clay type, and moisture. Although after purification (such as acid treatment), clay still contains a number of impurities, and the types of impurities vary greatly depending on the environment of clay deposit. Furthermore, according to previous reports, the size of clay filler in the composite electrolytes significantly affects their Li^+ conductivity, which is related to the Li^+ transport mechanism at the interface between the clay filler and the polymer matrix. Moreover, among different clays, 2D clay material, such as montmorillonite, has a unique layered structure, providing efficient Li^+ transport pathway with low energy barrier, and the composite SPE with which exhibited high Li^+ conductivity due to its wide and adjustable interlayer spacing. However, there is still little discussion the effects of different types of clay on stabilizing LMAs, which requires further efforts to prove and explore. In addition, it is easy for clays to absorb water which affects their electrochemical properties, but this aspect has rarely been investigated in LMBs. These above-mentioned influencing factors may lead to the uncertainty of the battery performance and restrict the industrialization of natural clay-based LMBs. Therefore, it is necessary to consider these influencing factors for the practical application of NCBMs in LMBs.

(2) New natural clay's modification method. Since existing clay modification methods still can not meet requirements of high-performance LMBs, efficient and low-cost modification methods of natural clays still need to be explored. In the previous reports, one of the most common modification strategies is ionic exchange, mainly including Li^+, Ag^{2+}, and Na^+. The ionic exchange can expand the interlayer spacing of natural clays, thereby promoting the migration of Li^+. Also, developing NCBMs that can *in-situ* form lithiophilic sites, is a promising strategy for promoting rapid and uniform lithium deposition. However, there is no doubt that the above strategy will increase the cost, especially for Ag^{2+} ionic exchange. Therefore, designing an efficient and low-cost modification method for natural clays is necessary, especially for large-scale applications, and how to balance electrochemical performance and cost still needs further study. Furthermore, to date, all of the reported modification strategies are still laboratory scale, and shifting from laboratory scale to industrial level remains great challenging.

(3) Mechanism exploration. NCBMs are used for stable LMAs, but the detailed mechanism remains unclear. For example, for composite SSEs, the Lewis acid sites of NCBMs are thought to play an important role in improving Li^+ conductivity and Li^+ transference number, but it lacks sufficient evidence. Furthermore, the solvation structure of Li^+ significantly affects its transport properties and deposition behavior, but this is rarely discussed in natural clay-based composite electrolytes. In this regard, *in situ* characterization techniques (*e.g.*, *in situ* X-ray characterization techniques, *in situ* TEM characterization, *in situ* Raman characterization), multiscale multi-physics (*e.g.*, ion concentration field, electric field, stress field, and temperature field) coupled theoretical simulations and calculations (*e.g.*, density functional theory calculations, molecular dynamics simulation)

may assist in revealing the potential failure mechanisms of lithium metal batteries and guide the exploration of high-performance natural clay-based LMBs.

(4) Practical applications. Although the research on natural clay-based LMBs have made great progress, there are still great challenges in their practical applications. For example, in order to obtain high energy-density LMBs, the cathodes with a high areal loading of active material is important. Also, the use of thin LMAs and lean LEs/thin SSEs are necessary to further improve the energy density of LMBs. Although NCBMs exhibit excellent electrochemical performance in LMBs, these excellent electrochemical properties are mainly based on laboratory-scale coin-type cells, which makes it difficult to prove the true potential of NCBMs in pouch cells. Therefore, it is necessary to evaluate the impact of NCBMs for stable LMAs in practical pouch cell.

Overall, this review provides a fundamental understanding and recent advances in NCBMs for stable LMAs. Although significant progress has been made, the research on NCBMs for stable LMAs is still in its early stages. We hope that this review will further promote the practical applications of NCBMs in high-performance LMAs.

Declaration of competing interest

The authors declare that they have no known competing financial interests or personal relationships that could have appeared to influence the work reported in this paper.

Acknowledgments

This work was supported by the Henan Province Science and Technology Research Project (No. 232102241006), the National Key Research and Development Program of China (No. 2020YFB1713500), Opening Project of National Joint Engineering Research Center for Abrasion Control and Molding of Metal Materials & Henan Key Laboratory of High-temperature Structural and Functional Materials, Henan University of Science and Technology (No. HKDNM2019013), the Open Fund of State Key Laboratory of Advanced Refractories (No. SKLAR202210), and the Major Science and Technology Projects of Henan Province (No. 221100230200).

References

[1] G. Ma, O.A. Syzgantseva, Y. Huang, et al., Nat. Commun. 14 (2023) 501.
[2] Z.P. Yao, Y.W. Lum, A. Johnston, et al., Nat. Rev. Mater. 8 (2023) 202–215.
[3] X.W. Chi, M.L. Li, J.C. Di, et al., Nature 592 (2021) 551–557.
[4] R. Chen, D.S. Butenko, S. Li, et al., Chin. Chem. Lett. 35 (2024) 108358.
[5] H. Zhao, W. Kang, N. Deng, et al., Chem. Eng. J. 384 (2020) 123312.
[6] J.W. Liu, D.X. Xie, W. Shi, et al., Chem. Soc. Rev. 49 (2020) 1624–1642.
[7] J.W. Jung, S.H. Cho, J.S. Nam, et al., Energy Stor. Mater. 24 (2020) 512–528.
[8] Z.Y. Tu, P. Nath, Y.Y. Lu, et al., Acc. Chem. Res. 48 (2015) 2947–2956.
[9] D.H. Han, M. Zhang, P.X. Lu, et al., J. Energy Chem. 52 (2021) 75–83.
[10] Y.B. He, Z. Chang, S.C. Wu, et al., J. Mater. Chem. A 6 (2018) 6155–6182.
[11] Z.D. Hao, Q. Zhao, J.D. Tang, et al., Mater. Horiz. 8 (2021) 12–32.
[12] Y.L. Jie, X.D. Ren, R.G. Cao, et al., Adv. Funct. Mater. 30 (2020) 1910777.
[13] J.L. Lang, L.H. Qi, Y.Z. Luo, et al., Energy Stor. Mater. 7 (2017) 115–129.
[14] R. Balasubramaniam, C.W. Nam, V. Aravindan, et al., ChemElectroChem 9 (2022) e202200317.
[15] R. Wang, W. Cui, F. Chu, et al., J. Energy Chem. 48 (2020) 145–159.
[16] Z.X. Liu, Y. Liu, Y.J. Miao, et al., Energy Environ. Mater. 6 (2023) e12525.
[17] Q.J. Yu, K.C. Jiang, C.L. Yu, et al., Chin. Chem. Lett. 32 (2021) 2659–2678.
[18] X.T. Yuan, A.A. Razzaq, Y.J. Chen, et al., Chin. Chem. Lett. 32 (2021) 890–894.
[19] B.X. Zhou, A. Bonakdarpour, I. Stosevski, et al., Prog. Mater Sci. 130 (2022) 100996.
[20] S. Park, H.J. Jin, Y.S. Yun, Adv. Mater. 32 (2020) 2002193.
[21] Y. Gao, B.F. Cui, J.J. Wang, et al., Rare Met. 41 (2022) 3391–3400.
[22] Q. Ke, Q. Xu, X. Lai, et al., Chin. Chem. Lett. 34 (2023) 107602.
[23] H.S. Wang, Z. Yu, X. Kong, et al., Joule 6 (2022) 588–616.
[24] W.Y. Wu, Y. Bai, X.R. Wang, et al., Chin. Chem. Lett. 32 (2021) 1309–1315.
[25] M. Yuan, K. Liu, J. Energy Chem. 43 (2020) 58–70.
[26] P.B. Zhai, L.X. Liu, X.K. Gu, et al., Adv. Energy Mater. 10 (2020) 2001257.
[27] Y. Lan, Y. Liu, J. Li, et al., Adv. Sci. 8 (2021) 2004036.
[28] H. Tang, M. Sun, C. Wang, Chem. Asian J. 16 (2021) 2842–2851.
[29] T.T. Zhang, W. Wang, Y.L. Zhao, et al., Chem. Eng. J. 420 (2021) 127574.
[30] Y. Nan, S. Li, C. Han, et al., Adv. Funct. Mater. 31 (2021) 2102336.
[31] W.Y. Li, Z.H. Luo, X. Long, et al., ACS Appl. Mater. Interfaces 13 (2021) 51107–51116.
[32] Q. Ma, X. Sun, P. Liu, et al., Angew. Chem. Int. Ed. 58 (2019) 6200–6206.
[33] J. Park, S. Ha, J.Y. Jung, et al., Adv. Sci. 9 (2022) 2104145.
[34] H. Liu, R. Tao, C. Guo, et al., Chem. Eng. J. 429 (2022) 132239.
[35] M. Yang, Y. Ji, Y. Dong, et al., Chin. Chem. Lett. 34 (2023) 107087.
[36] C. Guo, Z.H. Luo, M.X. Zhou, et al., Small 19 (2023) e2301428.
[37] L. Yang, X. Yang, F. Xia, et al., Chem. Asian J. 18 (2023) e202300473.
[38] E. Abu-Danso, S. Peraniemi, T. Leiviska, et al., J. Hazard. Mater. 381 (2020) 120871.
[39] A. Sheikhhosseini, M. Shirvani, H. Shariatmadari, Geoderma 192 (2013) 249–253.
[40] S. Komarneni, Clays Clay Miner. 37 (1989) 469–473.
[41] E. Padilla-Ortega, R. Leyva-Ramos, J. Mendoza-Barron, et al., Adsorpt. Sci. Technol. 29 (2011) 569–584.
[42] I. Anastopoulos, A. Mittal, M. Usman, et al., J. Mol. Liq. 269 (2018) 855–868.
[43] P. Yuan, P.D. Southon, Z.W. Liu, et al., J. Phys. Chem. C 112 (2008) 15742–15751.
[44] Q. Zhu, X. Wang, J.D. Miller, ACS Appl. Mater. Interfaces 11 (2019) 8954–8960.
[45] A.B. ElDeeb, V.N. Brichkin, M. Bertau, et al., Appl. Clay Sci. 196 (2020) 105771.
[46] Y.M. Jeon, S. Kim, M. Lee, et al., Adv. Energy Mater. 10 (2020) 2003114.
[47] Y.M. Gao, Y. Liu, K.J. Feng, et al., Rare Met. 43 (2024) 1–19.
[48] W. Tang, S. Tang, X. Guan, et al., Adv. Funct. Mater. 29 (2019) 1900648.
[49] W. Tang, S. Tang, C. Zhang, et al., Adv. Energy Mater. 8 (2018) 1800866.
[50] E. Ozmetin, M.M. Kocakerim, Desalin. Water Treat. 124 (2018) 279–286.
[51] V.I. Loganina, E.E. Simonov, W. Jezierski, et al., Constr. Build. Mater. 65 (2014) 29–37.
[52] N.S. Fu, S.H. Zhang, Y.Y. Ma, et al., RSC Adv. 10 (2020) 9808–9813.
[53] S. Barakan, V. Aghazadeh, Environ. Sci. Pollut. Res. 28 (2021) 2572–2599.
[54] H. Mao, Z. Ding, J. Mater. Sci. Mater. Electron. 31 (2020) 13874–13888.
[55] V.A.A. España, B. Sarkar, B. Biswas, et al., Environ. Technol. Innov. 13 (2019) 383–397.
[56] R. Novikau, G. Lujaniene, J. Environ. Manag. 309 (2022) 114685.
[57] H. Porthault, C. Calberg, J. Amiran, et al., J. Power Sources 482 (2021) 229055.
[58] L. Wu, Y. Yu, Y. Dai, et al., ChemSusChem 15 (2022) 2101991.
[59] H.B. Yan, S.M. Li, Y. Nan, et al., Adv. Energy Mater. 11 (2021) 2100186.
[60] K. Malachova, P. Praus, Z. Rybkova, et al., Appl. Clay Sci. 53 (2011) 642–645.
[61] Q.H. Kong, Y. Hu, L. Yang, et al., Polym. Compos. 27 (2006) 49–54.
[62] Q.Q. Hao, G.W. Wang, Y.H. Zhao, et al., Fuel 109 (2013) 33–42.
[63] F. He, W. Tang, X. Zhang, et al., Adv. Mater. 33 (2021) 2105329.
[64] X. Sun, X. Zhang, Q. Ma, et al., Angew. Chem. Int. Ed. 59 (2020) 6665–6674.
[65] J.M. Yassin, Y. Shiferaw, A. Tedla, Heliyon 8 (2022) e09241.
[66] L. Boudriche, R. Calvet, B. Hamdi, et al., Colloids Surf. A 392 (2011) 45–54.
[67] K.G. Bhattacharyya, S.S. Gupta, Adv. Colloid Interface Sci. 140 (2008) 114–131.
[68] Y.S. Ding, C.Y. Guo, J.Y. Dong, et al., J. Appl. Polym. Sci. 102 (2006) 4314–4320.
[69] R. Chen, F.B. Peng, S.P. Su, J. Appl. Polym. Sci. 108 (2008) 2712–2717.
[70] R. Mukhopadhyay, D. Bhaduri, B. Sarkar, et al., J. Hazard. Mater. 383 (2020) 121125.
[71] S.M. Chen, H.L. Gao, X.H. Sun, et al., Matter 1 (2019) 412–427.
[72] F. Gonzalez, P. Tiemblo, N. Garcia, et al., Membranes 8 (2018) 55.
[73] J.J. Liu, X.P. Li, S.L. Zuo, et al., Appl. Clay Sci. 37 (2007) 275–280.
[74] K. Kamada, J.H. Kang, S.M. Paek, et al., J. Phys. Chem. Solids 73 (2012) 1478–1482.
[75] S. Mnasri-Ghnimi, N. Frini-Srasra, Appl. Clay Sci. 179 (2019) 105151.
[76] L. Heller-Kallai, Handbook of Clay Science, Elsevier, Amsterdam, 2013, pp. 411–433.
[77] C. Maqueda, M.D. Afonso, E. Morillo, et al., Appl. Clay Sci. 72 (2013) 175–183.
[78] A. Mejia, S. Devaraj, J. Guzman, et al., J. Power Sources 306 (2016) 772–778.
[79] P. Yao, B. Zhu, H. Zhai, et al., Nano Lett. 18 (2018) 6113–6120.
[80] L. Chen, W. Li, L.Z. Fan, et al., Adv. Funct. Mater. 29 (2019) 1901047.
[81] J. Feng, X. Ao, Z. Lei, et al., Electrochim. Acta 340 (2020) 135995.
[82] Y. Wang, X. Li, Y. Qin, et al., Nano Energy 90 (2021) 106490.
[83] X. Li, Y. Wang, K. Xi, et al., Nanomicro Lett. 14 (2022) 210.
[84] X. Pei, J.L. Mu, J.H. Hong, et al., Appl. Clay Sci. 216 (2022) 106363.
[85] Y. Wang, K. Huang, P. Zhang, et al., Appl. Surf. Sci. 574 (2022) 151593.
[86] S. Lv, X. He, Z. Ji, et al., Adv. Energy Mater. 13 (2023) 2302711.
[87] L. Wang, S. Yi, Q. Liu, et al., Energy Stor. Mater. 63 (2023) 102961.
[88] Y. Zhang, J. Huang, H. Liu, et al., Adv. Energy Mater. 13 (2023) 2300156.
[89] Y. Zhao, L. Li, Y. Shan, et al., Small 19 (2023) e2301572.
[90] L. Zhang, X. Xu, S. Jiang, et al., J Colloid Interface Sci 645 (2023) 45–54.
[91] Y. Jing, Q. Lv, B. Wang, et al., Energy Stor. Mater. 65 (2024) 103109.
[92] T. Zeng, Y. Yan, M. He, et al., J. Mater. Chem. A 10 (2022) 23712–23721.
[93] Y. Feng, B. Zhong, R. Zhang, et al., Adv. Energy Mater. 13 (2023) 2203912.
[94] F. Zhou, Z. Li, Y.Y. Lu, et al., Nat. Commun. 10 (2019) 2482.
[95] W. Chen, Y. Hu, W. Lv, et al., Nat. Commun. 10 (2019) 4973.
[96] M. Yang, N. Jue, Y. Chen, et al., Nanoscale Res. Lett. 16 (2021) 52.
[97] Y. Zhai, X. Wang, Y. Chen, et al., J. Membr. Sci. 621 (2021) 118996.
[98] X.Q. Xu, R. Xu, X.B. Cheng, et al., J. Energy Chem. 56 (2021) 391–394.
[99] Z. Zhang, J. Wang, H. Qin, et al., ACS Nano 18 (2024) 2250–2260.
[100] H. Zhang, S. Wang, Y. Wang, et al., Chin. Chem. Lett. 34 (2023) 108031.
[101] M. Ge, X. Zhou, Y. Qin, et al., Chin. Chem. Lett. 33 (2022) 3894–3898.

[102] Q.Z. Zhong, B. Liu, B.J. Yang, et al., Chin. Chem. Lett. 32 (2021) 3496–3500.
[103] Q. Liu, L. Wang, X.M. He, Adv. Energy Mater. 13 (2023) 2300798.
[104] S.L. Gao, M.X. Zhang, C. Gainaru, et al., Matter 5 (2022) 2457–2460.
[105] Z. Shen, J. Zhong, J. Chen, et al., Chin. Chem. Lett. 34 (2023) 107370.
[106] S.X. Xia, C.W. Yang, Z.Y. Jiang, et al., Adv. Compos. Hybrid Mater. 6 (2023) 198.
[107] J. Zheng, M. Chen, H. Yuan, et al., Chin. Chem. Lett. (2023) 108812.
[108] L. Li, P. Ji, M. Huang, et al., Chin. Chem. Lett. 35 (2024) 109144.
[109] S. Ni, S. Tan, Q. An, et al., J. Energy Chem. 44 (2020) 73–89.
[110] H. Chen, M. Li, C. Li, et al., Chin. Chem. Lett. 33 (2022) 141–152.
[111] K.X. Liu, Z.Y. Wang, L.Y. Shi, et al., J. Energy Chem. 59 (2021) 320–333.
[112] H.P. Wu, L.B. Chen, Y.J. Chen, Sustain. Energy Fuels 5 (2021) 5656–5671.
[113] X. Han, T. Wu, L. Gu, et al., Chin. Chem. Lett. 34 (2023) 107594.